Journal of Alloys and Compounds 1083 (2026) 191699

Contents lists available at ScienceDirect

Journal of Alloys and Compounds

journal homepage: www.elsevier.com/locate/jalcom

Research article

Origin of the low thermal conductivity and thermal properties of $BaIn_2Te_4$

Bryson Winter [a], Hugo Bouteiller [b], Kaya Wei [c], Hsin Wang [b], George S. Nolas [a,*]

[a] Department of Physics, University of South Florida, Tampa, FL, 33620, USA
[b] Materials Science and Technology Division, Oak Ridge National Laboratory, Oak Ridge, TN, 37831, USA
[c] National High Magnetic Field Laboratory, Florida State University, Tallahassee, FL, 32310, USA

ARTICLE INFO

Keywords:
Ternary chalcogenide
Thermal properties
Lattice anharmonicity
Low thermal conductivity

ABSTRACT

Materials research involving multinary chalcogenide compositions for technologically significant applications continues to attract attention, and an understanding of the thermal properties of materials is essential for all technologically significant applications. Herein we report on an investigation of the structure-thermal property relationship of $BaIn_2Te_4$ and reveal the characteristics that govern the thermal properties of this ternary chalcogenide. Our analysis and modeling of the temperature-dependent thermal properties reveal a low speed of sound, low Debye temperature, and low thermal conductivity over a broad temperature range, attributable to lattice anharmonicity, large-mass constituent atoms and low-frequency optic modes. Our results provide new insights into the transport properties of the $BaIn_2Te_4$ ternary chalcogenide and further expand the exploration of metal chalcogenides for applications of technological interest.

1. Introduction

Multinary chalcogenides represent a class of materials that continue to be of interest as promising materials for nonlinear optics, photovoltaic, and thermoelectric applications. This is because they possess complex crystal structures that result in physical properties that can be tuned to improve performance. Recent studies report that specific chalcogenides have been developed to have wide optical transparency and high laser damage thresholds, which are of interest for applications in nonlinear optics [1,2], while certain multinary chalcogenides have shown promise for photovoltaic and photodetector technologies as they have been reported to exhibit direct bandgaps with high absorption coefficients allowing them to be candidate materials for solar cell applications [3–7]. In addition, certain multinary chalcogenides are of interest for both photovoltaic and thermoelectric applications [7–12].

Although the development of materials for technologically significant applications continues to intensify, an understanding of the thermal properties is essential. For example, thermal conductivity directly impacts performance in thermoelectrics [13], temperature sensitivity plays a critical role for photovoltaics [14,15], and the dissipation of heat prevents thermal gradients and can avoid birefringence effects [16]. An understanding of the thermal properties therefore allows for an understanding of the impact these properties have on performance during operating conditions in device applications [15]. Equally essential is the study of the fundamental thermal properties of matter; an understanding of thermal properties is a significant aspect of materials research.

The ternary II-III_2-VI_4 family of chalcogenide compounds encompasses many compositions [17–24]; however, there have only been a few reports on II-III_2-VI_4 compositions with the *Cccm* structure type [19,24]. The early work by Klee and Schäfer first uncovered such compositions with the TlSe structure [24], while Eisenmann *et al.* were the first to definitively determine the crystal structure of $BaIn_2Te_4$ [19]. More recently, Ishtiyak *et al.* revealed this ternary chalcogenide to be a semiconductor with very high resistivity and low thermal conductivity above 500 K [25]. In this work, we report on the structure and low-temperature thermal properties of $BaIn_2Te_4$, including temperature-dependent heat capacity and thermal conductivity over a large temperature range, revealing deviation from Debye behavior with low-energy optic modes and relatively high lattice anharmonicity resulting in thermal conductivity values that are lower than those of other multinary chalcogenides. These results support the fundamental understanding of this and related multinary chalcogenides given the ongoing interest in these materials for optical and optoelectronic applications, as knowledge of thermal properties is important for optical applications [14,15].

* Corresponding author.
E-mail address: gnolas@usf.edu (G.S. Nolas).

https://doi.org/10.1016/j.jallcom.2026.191699
Received 3 June 2026; Received in revised form 25 September 2026; Accepted 11 October 2026
Available online 16 October 2026
0925-8388/© 2026 Elsevier B.V. All rights are reserved, including those for text and data mining, AI training, and similar technologies.

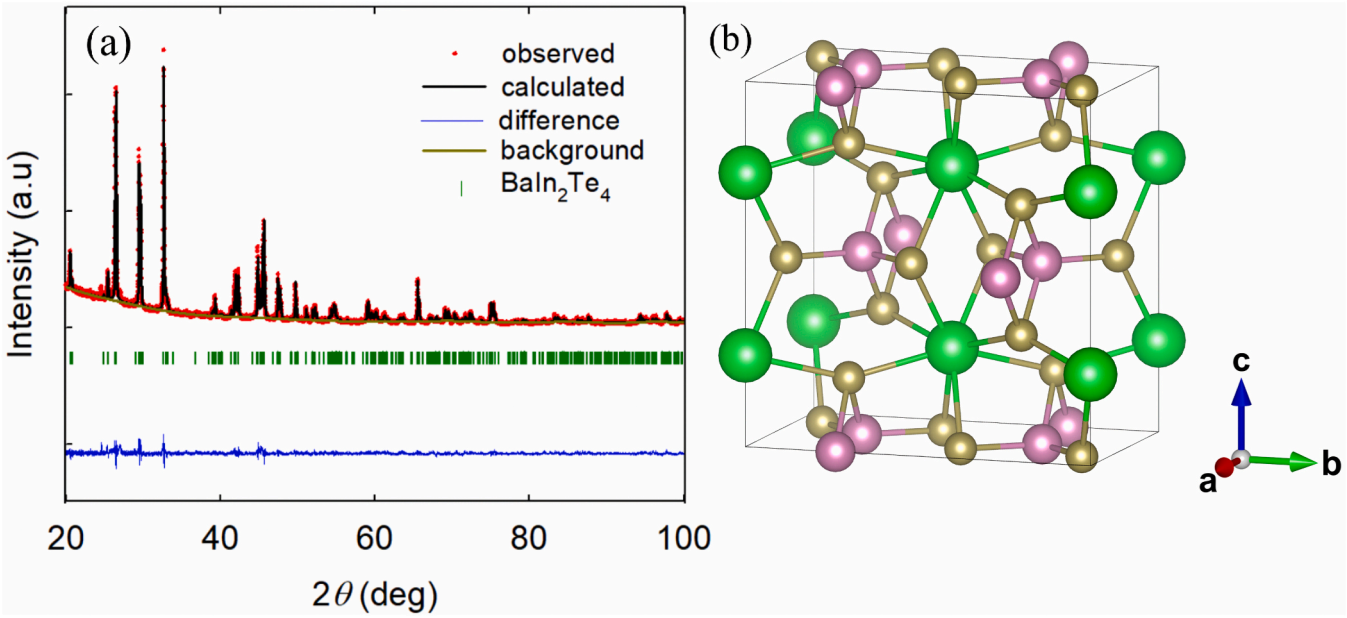


Fig. 1. (a) Powder XRD pattern including the profile fit, profile difference, and Bragg positions of $BaIn_2Te_4$. (b) Crystal structure of $BaIn_2Te_4$ viewed along the *a*-axis, drawn within the orthorhombic unit cell (space group *Cccm*, No. 66). The barium, indium and tellurium atoms are represented by green, pink and gold spheres, respectively.

2. Methodology

A modified synthesis process adapted from Ishtiyak *et al* [25]. was employed with an additional 3% by mass of Ba added during the homogenization process to eliminate the formation of In_2Te_3 impurity that was observed when the exact stoichiometric ratio was used to prepare $BaIn_2Te_4$. The mass of the excess Ba required was determined based on the amount of In_2Te_3 impurity present in the product after processing attempts when stoichiometric amounts of Ba were used. No excess BaO was identified in the bulk specimen as indicated by X-ray diffraction (XRD) data from different pieces of the pellet obtained after cutting the pellet for the different measurements reported in this study. High-purity samples of the constituent elements (Ba pieces, 99.2%; In shot, 99.99%; Te powder, 99.5%) were loaded into a BN crucible before being sealed in a quartz ampoule under vacuum using flame sealing. The ampoule was placed in a resistive furnace and heated to 1123 K at a rate of 25 K/h. After holding at this temperature for 0.5 h, the sample was cooled to 973 K at a rate of 50 K/h, and held for 96 h. The obtained product was ground in a N_2 glove box and cold-pressed into several pellets before being loaded into a BN crucible and repeating the above temperature profile. The product was then ground, sieved (325 mesh) and loaded into a custom-designed graphite die and molybdenum punch assembly that was then placed into a Thermal Technology LLC hot press. The sample was hot-pressed under a pressure of 160 MPa and a temperature of 598 K for 5 h in a continuously flowing N_2 atmosphere. A compact polycrystalline disc was obtained, with a density of 85% relative to the theoretical density as calculated from the mass and dimensions of the disc. Higher density pellets were obtained by adjusting the hot-pressing parameters; however, this also resulted in the formation of Te as an impurity within the bulk pellet and those pellets were not used for this study.

To confirm the structure of $BaIn_2Te_4$, XRD measurements were carried out using a Rigaku SmartLab X-ray Diffractometer in Bragg–Brentano geometry with Cu Kα radiation ($\lambda = 1.5418$ Å) and a graphite monochromator. Rietveld structural refinement was performed using GSAS II software. A MIRA3 TESCAN field-emission scanning electron microscope (SEM) was used, equipped with an APEX Octane Elite with energy-dispersive X-ray spectroscopy (EDS) detector to determine the stoichiometry, homogeneity, and grain size of the specimens. The composition determined using EDS was similar to that determined by Rietveld refinement of the XRD data. SEM backscattered electron (BSE) micrographs revealed a polycrystalline microstructure with grain sizes ranging from 2 to 20 μm.

A wire saw was used to cut the disc into specific dimensions, including $2 \times 2 \times 6$ mm^3 and $2 \times 2 \times 0.5$ mm^3 parallelepipeds for thermal conductivity and heat capacity measurements, respectively. Thermal conductivity, κ, was measured on a custom-designed radiation-shielded vacuum probe with a maximum experimental uncertainty of 8% [26,27]. Temperature-dependent isobaric heat capacity, C_p, was measured on a Quantum Design Physical Property Measurement System (PPMS) from 2 K to 250 K. The specimen was mounted on the sample

Table 1
Summary of Rietveld refinement results for the composition.

Nominal composition	$BaIn_2Te_4$
Space group, Z	*Cccm* (#66), 4
a (Å)	7.13593 (11)
b (Å)	12.02161 (12)
c (Å)	12.10720 (13)
α = β = γ (°)	90
V (Å^3)	1038.620 (16)
D_{calc} (g/cm^3)	5.6109
2θ range (°)	10–100
Step width (°)	0.01
wR_p, R_p	0.07725, 0.05399
Reduced χ^2	2.09

Table 2
Atomic coordinates and isotropic ADPs (Å^2) for $BaIn_2Te_4$.

atom	*site*	*x*	*y*	*z*	U_{iso}
Ba	*4b*	0	0	1/4	0.0425 (18)
In	*8 l*	0.5016 (14)	0.2434 (5)	0	0.0421 (14)
Te1	*8 l*	0.2424 (12)	0.06963 (28)	0	0.0361 (14)
Te2	*8k*	1/4	1/4	0.3211 (4)	0.0441 (15)

Table 3
Selected bond lengths and bond angles for the composition.

Bonding Atoms	Bond Lengths (Å) and Angles (°)
In – Te1	2.790 (10), 2.844 (10)
Ba – Te1	3.585 (4) × 4
In – Te2	2.800 (7) × 2
Ba – Te2	3.5994 (11) × 4
In – Te1 – In	79.3 (3)
Te1 – In – Te1	100.7 (3)

holder with Apiezon N-grease, and the addenda heat capacity data were independently measured and subtracted from the total signal. The maximum uncertainty in the entire temperature range was estimated to be 5%.

3. Results and discussion

Rietveld refinement confirmed that $BaIn_2Te_4$ adopts the orthorhombic space group *Cccm*, as shown in Fig. 1(a), with the refinement results summarized in Tables 1–3. The unit cell of $BaIn_2Te_4$ is shown in Fig. 1(b), and an image of a fractured surface of the specimen from SEM with EDS mapping of a polished specimen shown in Fig. 2. The structure adopts a pseudo-one-dimensional crystal structure built around $[In_2Te_4]$ chains propagating along the *a*-axis, with four such chains contained within each unit cell. The asymmetric unit comprises four distinct crystallographic sites: Ba at the 4*b* site, In at the 8 *l* site, Te1 at the 8 *l* site and Te2 at the 8*k* site. Each In atom is coordinated by two Te1 and two Te2 atoms in a distorted tetrahedral geometry, where the distortion of the $[InTe_4]$ units arises from steric effects. Adjacent $[InTe_4]$ tetrahedra

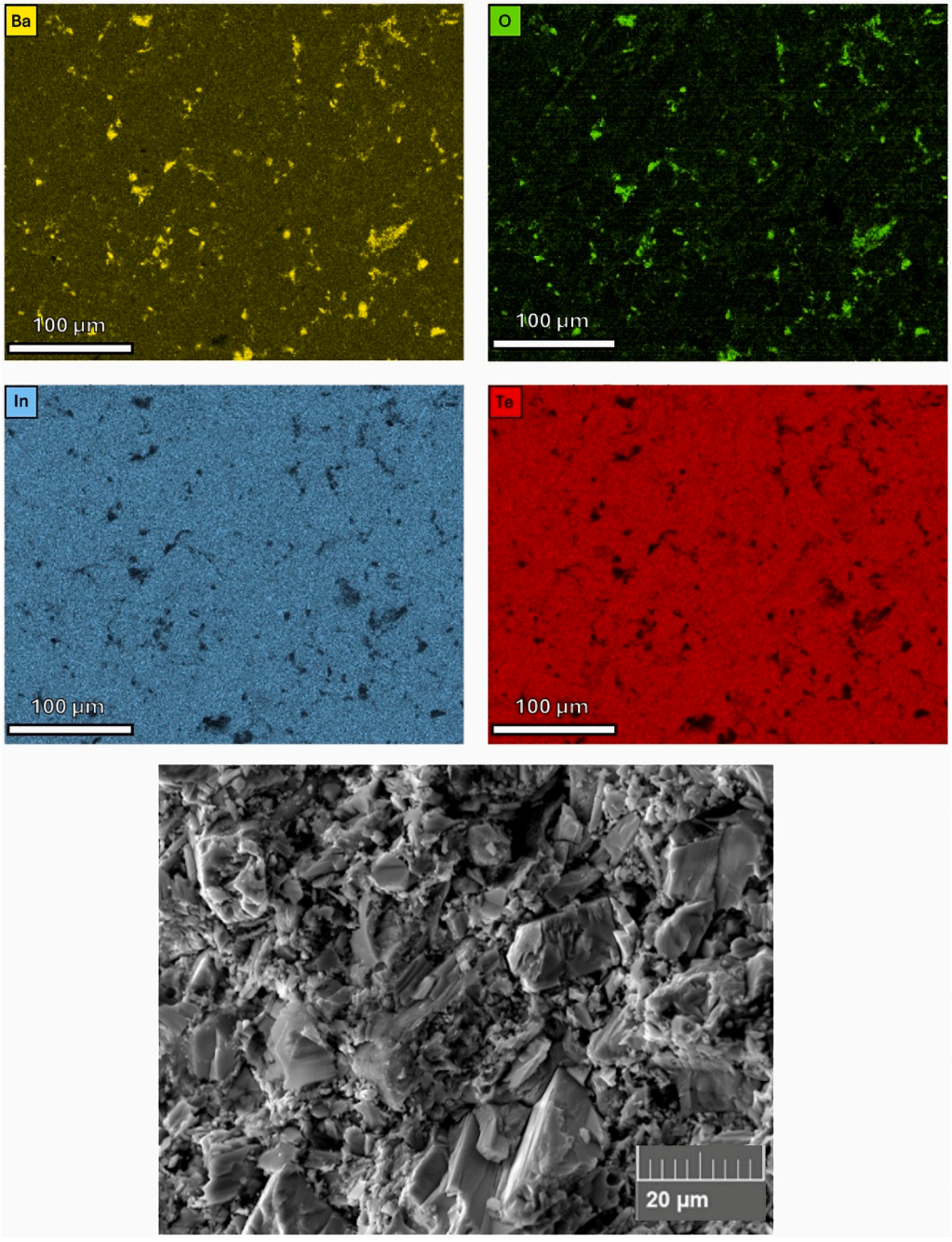


Fig. 2. EDS mapping of a polished surface of $BaIn_2Te_4$ with scale bars indicating 100 µm, and SEM-BSE image of a fractured surface of $BaIn_2Te_4$ with scale bar indicating 20 µm. The SEM image reveals a heterogeneous microstructure composed of irregularly shaped grains with an average grain size of 10 µm.

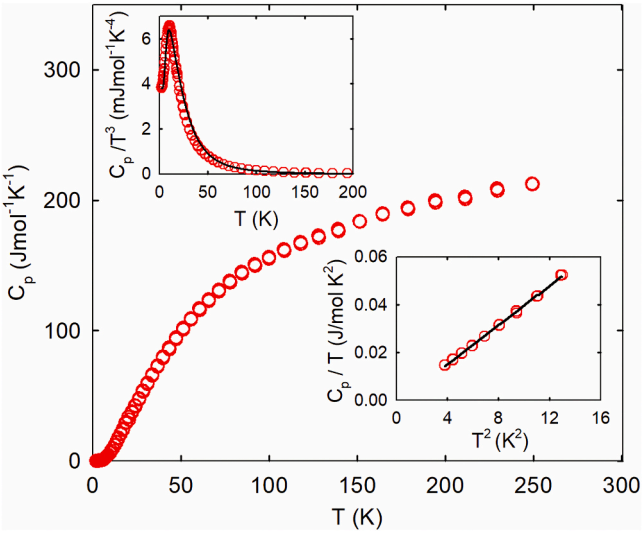


Fig. 3. Temperature-dependent heat capacity data. The bottom inset shows C_p/T as a function of T^2 at low temperatures with the solid line representing a fit of the form $C_p/T = \alpha + \beta T^2$, and the top inset shows the low-temperature C_p/T^3 data with the solid line representing a data fit to the model described in the text.

share two opposite edges to form the extended 1D chains along [100]. Barium cations reside within the tunnels defined by the surrounding [In_2Te_4] chains, where each Ba atom is coordinated by eight tellurium atoms arranged in a distorted square antiprism-like geometry. The In-Te bond lengths are approximately 2.8 Å, while the Ba-Te bond lengths of approximately 3.6 Å are notably longer, suggesting weaker bonding between Ba cations and the surrounding [$InTe_4$] framework. First-principles calculations by Gürel *et al.* indicate anisotropic properties in $BaIn_2Te_4$ [28], consistent with weak interchain Ba-Te interactions offering low resistance to shear deformations and transverse vibrations, which may inhibit thermal transport. The atomic displacement parameters (ADPs) of Ba and Te are similar, as shown in Table 2, and therefore do not support "rattling" behavior of the Ba cations.

To elucidate the thermal properties of this ternary chalcogenide, we first investigated the low-temperature C_p, as shown in Fig. 3. The Dulong-Petit limit is reached at above 140 K, suggesting that most vibrational modes are thermally activated above this temperature. The low-temperature data were fitted to the equation $C_p/T = \alpha + \beta T^2$, where C_p is isobaric heat capacity, T is temperature, α is the Sommerfeld coefficient, and β is the lattice contribution, as shown in the bottom inset of Fig. 3. Analysis of the fit yielded a Debye temperature, Θ_D, of 149 K and an average speed of sound, v, of 1673 m/s as determined using the expressions $\Theta_D = (12\pi^4 Rn/5\beta)^{1/3}$ and $v = (\Theta_D k_B/h)(3nN_a d/4\pi M)^{-1/3}$, where R is the ideal gas constant, n is the number of atoms per formula unit, k_B is Boltzmann's constant, h is Planck's constant, N_a is Avogadro's number, d is the density and M is the molecular weight [29]. The low Debye temperature and speed of sound can be attributed to heavy constituent atoms and weak bonding, with values that are comparable to that of other multinary chalcogenides with similar κ [30–32]. The obtained value for the Sommerfeld coefficient was close to zero, which is not surprising given the high resistivity reported for this material [25]. A plot of C_p/T^3 versus temperature, shown in the top inset of Fig. 3, indicates deviation from typical Debye behavior with a relatively large peak at $T_{max} \approx 10.5$ K, where T_{max} is the temperature at which the peak occurs, suggesting the presence of low-frequency vibrational modes. Using the relation $\Theta_E \approx 5T_{max}$ [33], an Einstein temperature of $\Theta_E \approx 52$ K was obtained. The early saturation of C_p is consistent with an abundance of low-frequency optical modes, as is also suggested from theoretical calculations [28], which can scatter acoustic phonons and contribute to suppressed thermal transport. To further investigate the thermal behavior, a phenomenological model that includes the Debye

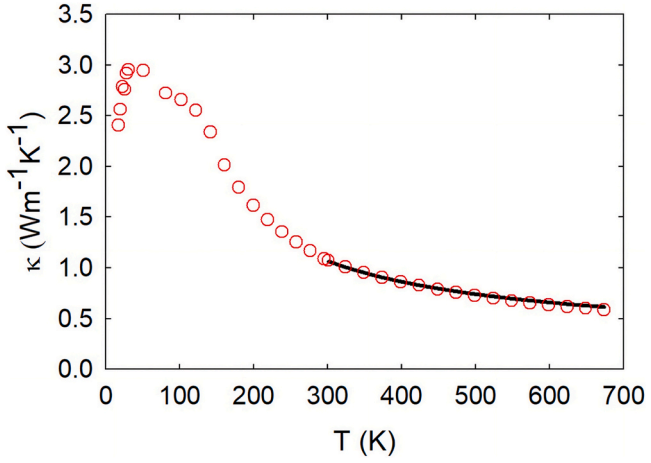


Fig. 4. Temperature-dependent κ data for 100% dense polycrystalline $BaIn_2Te_4$. The black solid line is proportional to $1/T$, indicative of the onset of Umklapp scattering at high temperatures.

and Einstein contributions was employed to analyze the C_p/T^3 data. The top inset to Fig. 3 shows the data fit to the model employing

$$C_p = \alpha T + AR\left(\frac{T}{\theta_D}\right)^3 \int_0^{\frac{\theta_D}{T}} \frac{x^4 e^x}{(e^x-1)^2} dx + BR\left(\frac{\theta_E}{T}\right)^2 \frac{\exp\left(\frac{\theta_E}{T}\right)}{\left(\exp\left(\frac{\theta_E}{T}\right)-1\right)^2} \quad (1)$$

where the terms in Eq. 1 represent the electronic contribution, Debye contribution, and Einstein contribution, respectively, and A and B are fitting parameters. All fitting parameters were uniquely determined using a minimization of the best sequence fit function, as compared to the data, and each of the terms was required to best fit the experimental data. From the fit, values of $\alpha = 0.001$ mJ mol^{-1} K^{-2}, $A = 54$, $\Theta_D = 145$ K, $B = 1.6$, and $\Theta_E = 48$ K, were obtained. The values of Θ_D and Θ_E from this fit agree well with the values obtained from the linear low-temperature C_p data and from the relation $\Theta_E \approx 5T_{max}$, respectively.

The κ data, shown in Fig. 4, indicate relatively low values at and above room temperature, and the excellent agreement between our high- and low-temperature κ data is an indication of the quality and homogeneity of the polycrystalline specimen synthesized for this study. Given the large electrical resistivity ($\rho \approx 25$ kΩ-cm at room temperature) for $BaIn_2Te_4$ [25] the κ values are primarily lattice contributions, with an estimate of the electronic contribution to κ obtained by the Wiedemann –Franz law, $\kappa_e = L_0 T/\rho$, where κ_e is the electronic contribution to thermal conductivity, and $L_0 = 2.44 \times 10^{-8}$ V^2/K^2. At room temperature, κ_e is 2.9×10^{-8} W/m·K and even at 675 K (where $\rho \approx 10$ Ω-cm) [25], κ_e is 1.6×10^{-4} W/m·K or 0.03% of the measured κ value. Moreover, to discern the effect of porosity, we incorporated a modified effective medium formulation [34] to estimate κ for 100% dense $BaIn_2Te_4$ from our measured data incorporating the effect from 15% porosity. Employing the expression $\kappa_{corrected} = \kappa_{measured}(2 + \Phi)/(2 - 2\Phi)$ [34], where $\kappa_{measured}$ is the measured κ data, $\kappa_{corrected} = \kappa$ for 100% dense $BaIn_2Te_4$, and Φ the porosity, the data shown in Fig. 4 incorporate the increase in κ for this porosity correction using $\Phi = 0.15$. These κ values are low and comparable to those of other low-κ multinary chalcogenides [30–32,35–39], *e.g.*, $MnIn_2Te_4$, $ZnIn_2Te_4$ and $Cs_2BaCu_8InTe_{10}$ with room-temperature κ values of between 1 W/m·K and 2 W/m·K. The peak in the κ data occurs at approximately 40 K, with grain boundary scattering dominating below this peak. As shown in the figure, the high-temperature data are in good agreement with the $1/T$ dependence for Umklapp scattering. Using the κ data and the results of the analyses described above, the Grüneisen parameter, γ, was estimated using the expression $\kappa = BMV^{1/3}\Theta_D^3/n^{2/3}\gamma^2 T$, where $B = 2.43 \times 10^{-8}/(1 - 0.514/\gamma + 0.228/\gamma^2)$, M is the average mass of an atom in the material, V

is the average volume per atom, and n is the number of atoms in the primitive cell [40–42]. Employing this equation a value of $\gamma = 1.7$ was obtained indicating relative anharmonicity for $BaIn_2Te_4$. This γ value is comparable to that of other multinary chalcogenides with similar κ, such as $AgInTe_2$ ($\gamma = 2$) and $CuZn_2InTe_4$ ($\gamma = 1.8$) but lower than that for chalcogenides with lower κ, such as $CuIn_2Se_4$ ($\gamma = 2.9$) [30,32,36,43]. These results agree with reported theoretical calculations that suggest a relatively large Grüneisen parameter and low-frequency optical modes in $BaIn_2Te_4$ [28].

4. Conclusion

Polycrystalline $BaIn_2Te_4$ was synthesized and the low-temperature thermal properties were investigated. A peak in C_p/T^3 data at ~ 10.5 K indicated an abundance of low-frequency vibrational modes, while the early saturation of C_p indicated a low Debye temperature and speed of sound as confirmed by analyses and modeling of the temperature-dependent data. The κ data were low relative to other multinary chalcogenides due to lattice anharmonicity as well as heavy constituent atoms. Although κ is low, the very high resistivity values preclude this material for potential thermoelectric applications. These findings establish $BaIn_2Te_4$ as an intrinsically low-thermal-conductivity multinary chalcogenide and should motivate broader exploration of the "AM_2X_4" family of compounds for technological applications of interest.

CRediT authorship contribution statement

Bryson Winter: Writing – original draft, Visualization, Validation, Investigation, Formal analysis, Data curation. **Hugo Bouteiller:** Data curation. **Kaya Wei:** Data curation. **Hsin Wang:** Data curation. **George S. Nolas:** Writing – review & editing, Supervision, Resources, Project administration, Methodology, Conceptualization.

Declaration of Competing Interest

The authors declare that they have no known competing financial interests or personal relationships that could have appeared to influence the work reported in this paper.

Acknowledgements

K.W. acknowledges the National High Magnetic Field Laboratory is supported by the National Science Foundation through NSF/DMR-2128556 and the State of Florida. H.W. acknowledges the support of the U.S. Department of Energy, Vehicle Technologies Office, Powertrain Materials Core Program and the International Energy Agency (IEA) Advanced Materials for transportation (AMT) Technology Collaboration Programme (TCP). Oak Ridge National Laboratory is managed by UT-Battelle LLC under contract DE-AC05000OR22725. H.B. is supported by the UT-ORII program managed by ORNL's director research and development (DRD) program.

References

[1] Y.Z. Huang, H. Zhang, C.S. Lin, W.D. Cheng, Z. Guo, G.L. Chai, $PbGa_2GeS_6$: an infrared nonlinear optical material synthesized by an intermediate-temperature self-fluxing method, Cryst. Growth & Des. 18 (2) (2018) 1162–1167, https://doi.org/10.1021/acs.cgd.7b01586.

[2] F. Liang, L. Kang, Z. Lin, Y. Wu, Mid-infrared nonlinear optical materials based on metal chalcogenides: structure–property relationship, Cryst. Growth & Des. 17 (4) (2017) 2254–2289, https://doi.org/10.1021/acs.cgd.7b00214.

[3] Y. Guo, X. Li, K. Feng, C. Li, M. Zhou, Y. Wu, J. Yao, $Li_7Cd_{4.5}Ge_4Se_{16}$ and $Li_{6.4}Cd_{4.8}Sn_4Se_{16}$: Strong Nonlinear Optical Response in Quaternary Diamond-Like Selenide Networks, Chem. Asian J. 13 (7) (2018) 871–876, https://doi.org/10.1002/asia.201800090.

[4] P. Feng, J.X. Zhang, M.Y. Ran, X.T. Wu, H. Lin, Q.L. Zhu, Rare-earth-based chalcogenides and their derivatives: an encouraging IR nonlinear optical material candidate, Chem. Sci. 15 (16) (2024) 5869–5896, https://doi.org/10.1039/D4SC00697F.

[5] P. Feng, S.H. Zhou, M.Y. Ran, B. Li, X.T. Wu, H. Lin, Q.L. Zhu, Isovalent cation substitution drives structural transformation and infrared nonlinear optical activity in Eu-based chalcogenides, Inorg. Chem. Front. 12 (7) (2025) 2648–2660, https://doi.org/10.1039/D4QI03346A.

[6] S.A. Vanalakar, P.S. Patil, J.H. Kim, Recent advances in synthesis of Cu_2FeSnS_4 materials for solar cell applications: a review, Sol. Energy Mater. Sol. Cells 182 (2018) 204–219, https://doi.org/10.1016/j.solmat.2018.03.021.

[7] R.S. Devika, P. Vengatesh, T.S. Shyju, Review on ternary chalcogenides: potential photoabsorbers, Mater. Today. Proc. (2023), https://doi.org/10.1016/j.matpr.2023.04.113.

[8] M.L. Liu, F.Q. Huang, L.D. Chen, I.W. Chen, A wide-band-gap p-type thermoelectric material based on quaternary chalcogenides of Cu_2ZnSnQ_4 (Q = S, Se), Appl. Phys. Lett. 94 (20) (2009), https://doi.org/10.1063/1.3130718.

[9] M. Ibáñez, R. Zamani, A. LaLonde, D. Cadavid, W. Li, A. Shavel, J. Arbiol, J. R. Morante, S. Gorsse, G.J. Snyder, A. Cabot, $Cu_2ZnGeSe_4$ nanocrystals: synthesis and thermoelectric properties, J. Am. Chem. Soc. 134 (9) (2012) 4060–4063, https://doi.org/10.1021/ja211952z.

[10] Y. Dong, H. Wang, G.S. Nolas, Synthesis, Crystal Structure, and High Temperature Transport Properties of p-Type $Cu_2Zn_{1-x}Fe_xSnSe_4$, Inorg. Chem. 52 (24) (2013) 14364–14367, https://doi.org/10.1021/ic402455x.

[11] K. Wei, L. Beauchemin, H. Wang, W.D. Porter, J. Martin, G.S. Nolas, Enhanced thermoelectric properties of $Cu_2ZnSnSe_4$ with Ga-doping, J. Alloy. Compd. 650 (2015) 844–847, https://doi.org/10.1016/j.jallcom.2015.08.046.

[12] C.K. Miskin, S.D. Deshmukh, V. Vasiraju, K. Bock, G. Mittal, A. Dubois-Camacho, S. Vaddiraju, R. Agrawal, Lead chalcogenide nanoparticles and their size-controlled self-assemblies for thermoelectric and photovoltaic applications, ACS Appl. Nano Mater. 2 (3) (2019) 1242–1252, https://doi.org/10.1021/acsanm.8b02125.

[13] H.J. Goldsmid, Improving the thermoelectric figure of merit, Sci. Technol. Adv. Mater. 22 (1) (2021) 280–284, https://doi.org/10.1080/14686996.2021.1903816.

[14] C. Sun, Y. Zou, C. Qin, B. Zhang, X. Wu, Temperature effect of photovoltaic cells: a review, Adv. Compos. Hybrid. Mater. 5 (4) (2022) 2675–2699, https://doi.org/10.1007/s42114-022-00533-z.

[15] L.M. Shaker, A.A. Al-Amiery, M.M. Hanoon, W.K. Al-Azzawi, A.A.H. Kadhum, Examining the influence of thermal effects on solar cells: a comprehensive review, Sustain. Energy Res. 11 (1) (2024) 6, https://doi.org/10.1186/s40807-024-00100-8.

[16] P. Singh, N.M. Ravindra, Temperature dependence of solar cell performance—an analysis, Sol. Energy Mater. Sol. Cells 101 (2012) 36–45, https://doi.org/10.1016/j.solmat.2012.02.019.

[17] E.R. Franke, H. Schäfer, Zur Strukturchemie ternärer Telluride der Alkali-und Erdalkalimetalle mit den Elementen der 3. Hauptgruppe/On the Structural Chemistry of Ternary Tellurides of Alkali-and Earthalkalimetalls with the Group-(III)-Elements, Z. F. üR. Naturforsch. B 27 (11) (1972) 1308–1315, https://doi.org/10.1515/znb-1972-1105.

[18] P. Dotzel, E. Franke, H. Schäfer, G. Schön, Zur Kenntnis von $MgAl_2Te_4$, $MgGa_2Te_4$ und $MgIn_2Te_4$/On the Ternary Tellurides $MgAl_2Te_4$, $MgGa_2Te_4$ and $MgIn_2Te_4$, Z. F. üR. Naturforsch. B 30 (3–4) (1975) 179–182, https://doi.org/10.1515/znb-1975-3-409.

[19] B. Eisenmann, M. Jakowski, H. Schäfer, Neue ternaere Varianten der TlSeStruktur: zur Kenntnis von $BaAl_2Te_4$(II), $SrGa_2Te_4$(II), $Srln_2Te_4$(II) und $Baln_2Te_4$(II), Rev. De. Chim. Miner. 19 (1982) 263–273. http://pascal-francis.inist.fr/vibad/index.php?action=getRecordDetail&idt=PASCAL83X0105726.

[20] M.Y. Kim, W.T. Kim, M.S. Jin, S.A. Park, S.H. Choe, C.I. Lee, S.C. Hyun, C.D. Kim, Impurity optical absorption of Co^{2+}-doped $BaGa_2S_4$, $BaGa_2Se_4$, $BaIn_2S_4$, and $BaIn_2Se_4$ single crystals, J. Phys. Chem. Solids 64 (4) (2003) 625–629, https://doi.org/10.1016/S0022-3697(02)00363-3.

[21] T. Takizawa, M. Kubo, C. Hidaka, Single crystal growth of $SrIn_2VI_4$ (VI = S, Se) compounds solidifying through supercooling, J. Cryst. Growth 275 (1–2) (2005) e433–e437, https://doi.org/10.1016/j.jcrysgro.2004.11.015.

[22] O. Madelung, II-III_2-VI_4 compounds. Semiconductors: Data Handbook, Springer Berlin Heidelberg, Berlin, Heidelberg, 2004, pp. 373–396.

[23] X. Jiang, W.R. Lambrecht, Electronic band structure of ordered vacancy defect chalcopyrite compounds with formula II-III_2-VI_4, Phys. Rev. B 69 (3) (2004) 035201, https://doi.org/10.1103/PhysRevB.69.035201.

[24] W. Klee, H. Schäfer, $CaAl_2Se_4$ und $SrAl_2Se_4$—Strukturvarianten des TlSe-Type/$CaAl_2Se_4$ and $SrAl_2Se_4$-Variants of the TlSe-Structure, Z. F. üR. Naturforsch. B 33 (8) (1978) 829–833, https://doi.org/10.1515/znb-1978-0803.

[25] M. Ishtiyak, S. Jana, S. Narayanswamy, A.K. Nishad, G. Panigrahi, P. P. Bhattacharjee, J. Prakash, Intrinsic extremely low thermal conductivity in $BaIn_2Te_4$: Synthesis, crystal structure, Raman spectroscopy, optical, and thermoelectric properties, J. Alloy. Compd. 802 (2019) 385–393, https://doi.org/10.1016/j.jallcom.2019.06.036.

[26] J. Martin, G.S. Nolas, Apparatus for the measurement of electrical resistivity, Seebeck coefficient, and thermal conductivity of thermoelectric materials between 300 K and 12 K, Rev. Sci. Instrum. 87 (1) (2016) 015105, https://doi.org/10.1063/1.4939555.

[27] J. Martin, S. Erickson, G.S. Nolas, P. Alboni, T.M. Tritt, J. Yang, Structural and transport properties of $Ba_8Ga_{16}Si_xGe_{30-x}$ clathrates, J. Appl. Phys. 99 (4) (2006) 044903, https://doi.org/10.1063/1.2171775.

[28] T. Gürel, Y.A. Altunay, P. Bulut, S. Yıldırım, C. Sevik, Comprehensive investigation of the extremely low lattice thermal conductivity and thermoelectric properties of $BaIn_2Te_4$, Phys. Rev. B 106 (19) (2022) 195204, https://doi.org/10.1103/PhysRevB.106.195204.

[29] C. Kittel, P. McEuen, Introduction to solid state physics, John Wiley & Sons, 2018.

[30] P. Qiu, Y. Qin, Q. Zhang, R. Li, J. Yang, Q. Song, Y. Tang, S. Bai, X. Shi, L. Chen, Intrinsically high thermoelectric performance in $AgInSe_2$ n-type diamond-like compounds, Adv. Sci. 5 (3) (2018) 1700727, https://doi.org/10.1002/advs.201700727.

[31] T. Suriwong, K. Kurosaki, S. Thongtem, A. Harnwunggmoung, T. Plirdpring, T. Sugahara, Y. Ohishi, H. Muta, S. Yamanaka, Synthesis and thermal conductivities of $ZnIn_2Te_4$ and $CdIn_2Te_4$ with defect-chalcopyrite structure, J. Alloy. Compd. 509 (27) (2011) 7484–7487, https://doi.org/10.1016/j.jallcom.2011.04.086.

[32] D. Hobbis, W. Shi, A. Popescu, K. Wei, R.E. Baumbach, H. Wang, L.M. Woods, G. S. Nolas, Synthesis, transport properties and electronic structure of p-type $Cu_{1+x}Mn_{2-x}InTe_4$ (x = 0, 0.2, 0.3), Dalton Trans. 49 (7) (2020) 2273–2279, https://doi.org/10.1039/C9DT04069B.

[33] E.A. Bensen, K. Ciesielski, L.C. Gomes, B.R. Ortiz, J. Falke, O. Pavlosiuk, D. Weber, T.L. Braden, K.X. Steirer, D. Szymański, J.E. Goldberger, Anomalous electronic properties in layered, disordered ZnVSb, Phys. Rev. Mater. 5 (1) (2021) 015002, https://doi.org/10.1103/PhysRevMaterials.5.015002.

[34] H. Lee, D. Vashaee, D.Z. Wang, M.S. Dresselhaus, Z.F. Ren, G. Chen, Effects of nanoscale porosity on thermoelectric properties of SiGe, J. Appl. Phys. 107 (9) (2010) 094308, https://doi.org/10.1063/1.3388076.

[35] O. Shahid, M. Ishtiyak, S.S. Rout, K.V. Ramanujachary, M.K. Niranjan, J. Prakash, Syntheses, crystal structures, and physical properties of non-centrosymmetric $MgIn_2Te_4$ and $MnIn_2Te_4$, Solid. State Sci. 152 (2024) 107552, https://doi.org/10.1016/j.solidstatesciences.2024.107552.

[36] O.P. Ojo, W.D. Gunatilleke, H. Wang, G.S. Nolas, Structural and thermal properties and the origin of the ultralow thermal conductivity in the defect stannite $CuIn_2Se_4$, Scr. Mater. 258 (2025) 116518, https://doi.org/10.1016/j.scriptamat.2024.116518.

[37] H. Nautiyal, K. Lohani, B. Mukherjee, E. Isotta, M.A. Malagutti, N. Ataollahi, I. Pallecchi, M. Putti, S.T. Misture, L. Rebuffi, P. Scardi, Mechanochemical synthesis of sustainable ternary and quaternary nanostructured Cu_2SnS_3, Cu_2ZnSnS_4, and $Cu_2ZnSnSe_4$ chalcogenides for thermoelectric applications, Nanomaterials 13 (2) (2023) 366, https://doi.org/10.3390/nano13020366.

[38] D. Zhang, H.C. Bai, Z.L. Li, J.L. Wang, G.S. Fu, S.F. Wang, Multinary diamond-like chalcogenides for promising thermoelectric application, Chin. Phys. B 27 (4) (2018) 047206, https://doi.org/10.1088/1674-1056/27/4/047206.

[39] R. Patschke, X. Zhang, D. Singh, J. Schindler, C.R. Kannewurf, N. Lowhorn, T. Tritt, G.S. Nolas, M.G. Kanatzidis, Thermoelectric properties and electronic structure of the cage compounds $A_2BaCu_8Te_{10}$ (A= K, Rb, Cs): systems with low thermal conductivity, Chem. Mater. 13 (2) (2001) 613–621, https://doi.org/10.1021/cm000390o.

[40] D.T. Morelli, G.A. Slack, in: S.L. Shindé, J.S. Goela (Eds.), High Thermal Conductivity Materials, Springer, New York, NY, 2006, pp. 37–68.

[41] G.A. Slack, in: H. Ehrenreich, F. Seitz, D. Turnbull (Eds.), Solid State Physics, 34, Academic Press, 1979, pp. 1–71.

[42] C.L. Julian, Theory of heat conduction in rare-gas crystals, Phys. Rev. 137 (1A) (1965) A128, https://doi.org/10.1103/PhysRev.137.A128.

[43] L. Ma, W. Shi, L.M. Woods, Structural diversity of $CuZn_2InSe_4$ quaternary chalcogenides: electronic and phonon properties from first principles, RSC Adv. 12 (41) (2022) 26648–26656, https://doi.org/10.1039/d2ra04261d.